PNAS RESEARCH ARTICLE | SUSTAINABILITY SCIENCE

Climate drives coupled regime shifts across subtropical estuarine ecosystems

Stephen G. Hesterberg[a,1,2], Kendal Jackson[b], and Susan S. Bell[a]

Edited by Garry Peterson, Stockholms Universitet, Stockholm, Sweden; received November 29, 2021; accepted June 21, 2022, by Editorial Board Member Ruth DeFries

Ecological regime shifts are expected to increase this century as climate change propagates cascading effects across ecosystems with coupled elements. Here, we demonstrate that the climate-driven salt marsh–to–mangrove transition does not occur in isolation but is linked to lesser-known oyster reef–to–mangrove regime shifts through the provision of mangrove propagules. Using aerial imagery spanning 82 y, we found that 83% of oyster reefs without any initial mangrove cover fully converted to mangrove islands and that mean (± SD) time to conversion was 29.1 ± 9.6 y. In situ assessments of mangrove islands suggest substantial changes in ecosystem structure during conversion, while radiocarbon dates of underlying reef formation indicate that such transitions are abrupt relative to centuries-old reefs. Rapid transition occurred following release from freezes below the red mangrove (*Rhizophora mangle*) physiological tolerance limit (−7.3 °C) and after adjacent marsh-to-mangrove conversion. Additional nonclimate-mediated drivers of ecosystem change were also identified, including oyster reef exposure to wind-driven waves. Coupling of regime shifts arises from the growing supply of mangrove propagules from preceding and adjacent marsh-to-mangrove conversion. Climate projections near the mangrove range limit on the Gulf coast of Florida suggest that regime shifts will begin to transform subtropical estuaries by 2070 if propagule supply keeps pace with predicted warming. Although it will become increasingly difficult to maintain extant oyster habitat with tropicalization, restoring oyster reefs in high-exposure settings or active removal of mangrove seedlings could slow the coupled impacts of climate change shown here.

climate change | *Crassostrea virginica* | historical ecology | mangrove | oyster reef

Significance

Climate change is reshaping entire ecosystems in sudden, unpredictable ways, but even more rapid change could occur this century due to unforeseen coupled elements between ecosystems. We follow the fate of oyster reefs over 82 y in an increasingly tropical estuary and provide empirical support for cascading regime shifts driven by climate. We find evidence of rapid and accelerating oyster reef–to–mangrove island conversion following climate release from severe winter freezes and adjacent marsh-to-mangrove transition. If propagule supply keeps pace with warming, we anticipate managers will face difficult choices on whether to accept, prevent, or modify rapid, landscape-wide ecosystem shifts in subtropical estuaries this century due to unforeseen coupling of marsh-to-mangrove and oyster reef–to–mangrove regime shifts.

Regime shifts, or the reorganization of a system's state from one stable equilibrium to another (1), are becoming increasingly apparent across social-ecological networks as human activity continues to impact profoundly the biosphere (2, 3). Whole ecosystem change can be abrupt, resulting from external stressors that dissolve ecological resilience to the point where only small changes in external drivers can produce rapid reconfigurations (4). Once novel states appear, they are often difficult to reverse due to internal feedbacks that reinforce the new regime and require human interventions to recover (5, 6).

Climate change threatens to propel an increasing number of ecosystems across critical transitions this century (7–9), as temperature influences core ecological processes across scales and is global in reach (9–11). With ecosystems closely coupled to macroclimate, it is anticipated that climate change will propagate multiple tipping dynamics or cascading regime shifts, where one climate-induced regime shift triggers another due to interactive elements (12–15). To date, such interactions remain largely conceptual but pose threats for rapid, landscape-wide ecological change (14). Here, we document how the release from extreme winter freezes, a well-established macroclimatic driver of the salt marsh–to–mangrove regime shift (16–18), also propagates a spatially adjacent regime shift by which oyster (*Crassostrea virginica*) reefs are replaced by red mangroves (*Rhizophora mangle*) to create forested islands. We also show that such climate-driven regime shifts will alter subtropical estuarine landscapes by the end of the present century and discuss implications of cascading regime shifts for coastal management.

We examined the dynamics of oyster reef–to–mangrove regime shifts in the shallow, subtropical landscape of Tampa Bay, FL, a large (>1,000 km^2) estuary on Florida's west-central Gulf coast (Fig. 1*A*) that has experienced tropicalization. Over the past 160 y, tidal wetlands in Tampa Bay have shifted from herbaceous to woody plant dominance, with an estimated 72% of salt marsh replaced by mangroves by 2000 relative to a 19th-century baseline (19). This tidal wetland conversion was nearly complete by the 1980s, following mosquito ditching of wetlands beginning in the 1950s (20). The well-understood magnitude and timing of historic mangrove encroachment in coastal landscapes of Tampa Bay provide a unique opportunity to examine past changes in

Author contributions: S.G.H. and S.S.B. designed research; S.G.H. and K.J. performed research; S.G.H. and K.J. contributed new reagents/analytic tools; S.G.H. and K.J. analyzed data; and S.G.H. and S.S.B. wrote the paper.

The authors declare no competing interest.

This article is a PNAS Direct Submission. G.P. is a guest editor invited by the Editorial Board.

[1]To whom correspondence may be addressed. Email: hesterberg@usf.edu.

[2]Present address: Gulf Shellfish Institute, 13230 Eastern Ave, Palmetto, FL 34221.

This article contains supporting information online at http://www.pnas.org/lookup/suppl/doi:10.1073/pnas.2121654119/-/DCSupplemental.

Published August 8, 2022.

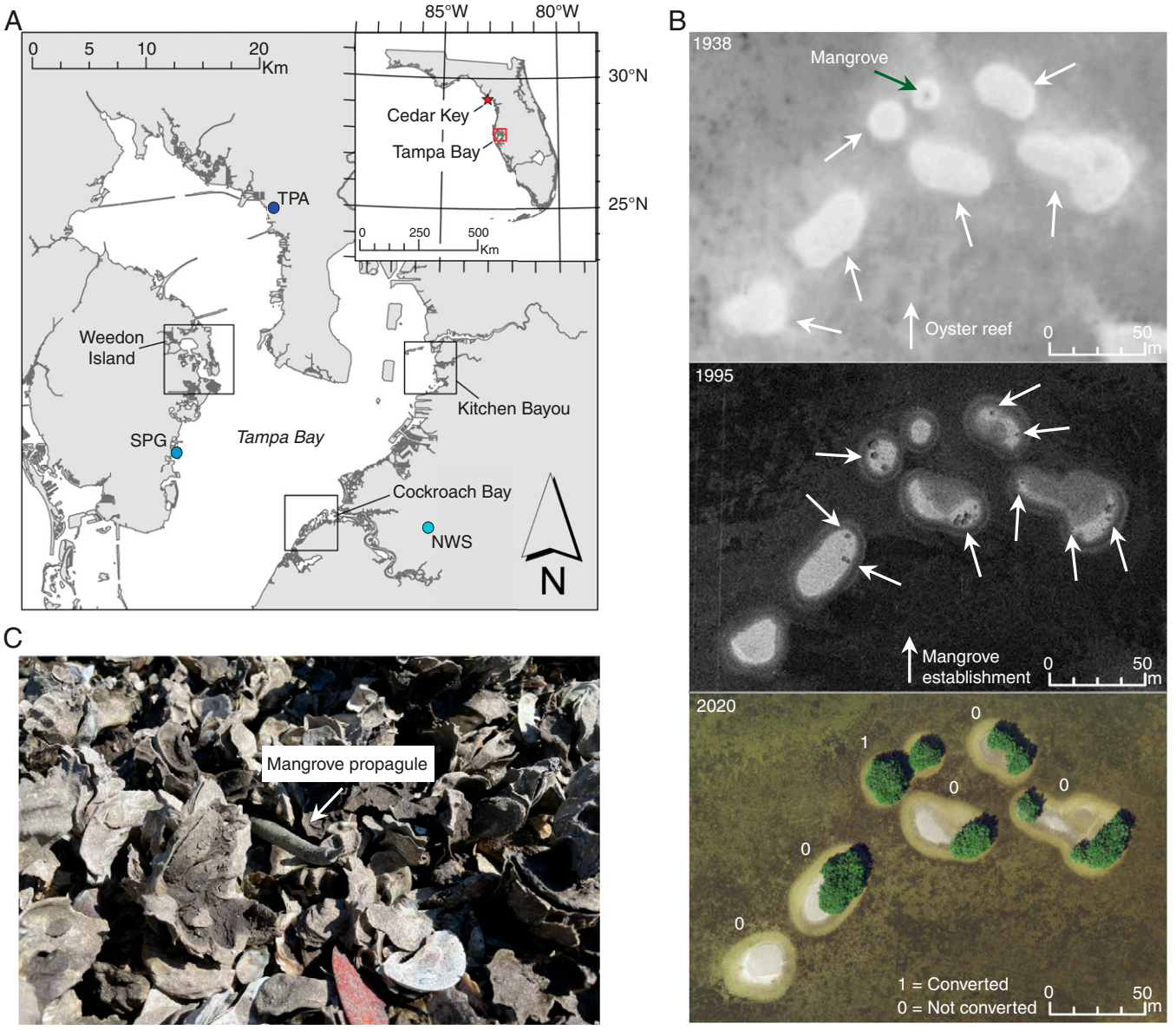

Fig. 1. Oyster reef–to–mangrove regime shifts from 1938 to 2020 in Tampa Bay, FL. (*A*) Map showing the location of three study areas within Tampa Bay: Cockroach Bay (CB), Kitchen Bayou (KB), and Weedon Island (WI), displaying dynamics of oyster reef–to–mangrove regime shifts. Climate records used in this study were obtained from local weather stations across Tampa Bay, and are indicated in *A* with points. Insert shows location of Tampa Bay in relation to Cedar Key, FL, the putative poleward range limit for *Rhizophora mangle* along Florida's west coast in 2020. (*B*) Example of aerial imagery used to track the fate of 111 oyster reefs over 82 y and quantify mangrove establishment, expansion, and conversion at subdecadal intervals (*SI Appendix*, Table S1). (*C*) Oyster reef with a recently established red mangrove (*R. mangle*) propagule. For a mangrove island to form, propagules must disperse from outside the oyster reef system and successfully establish within the interstices formed by oyster shells. NWS, National Weather Service; SPG, Albert Whitted Airport (St. Petersburg); TPA, Tampa International Airport. Image credit: S. G. Hesterberg, University of South Florida.

adjacent coastal ecosystems and use such observations to generate predictions of future oyster reef conversion as mangroves expand their distribution poleward.

At three sites within Tampa Bay, we recorded the fate of individual oyster reefs during historical mangrove expansion using aerial imagery (Fig. 1 and *SI Appendix*, Table S1). We examined oyster density and sedimentary records from select oyster reef and mangrove features to obtain in situ evidence of persistent and abrupt ecosystem change consistent with a regime shift (1). We then investigated these past regime shifts in the context of local climate and aspects of physical setting to elucidate drivers of mangrove establishment, expansion, and takeover on oyster reefs. Finally, we used our historical observations in Tampa Bay to predict the timing of oyster reef–to–mangrove regime shifts in response to climate warming at a northerly site, Cedar Key, FL, on Florida's Gulf coast (Fig. 1*A*), representing a location near the purported geographic range limit for the red mangrove (17).

Results and Discussion

Of the 111 oyster reefs identified without mangrove cover in the earliest aerial imagery, greater than 80% fully converted to mangrove islands, with proportional oyster reef survivorship at 0.168 after 82 y (Fig. 2*A*). Only three oyster reefs persisted without mangrove cover over the study period. Mangrove establishment on oyster reefs was best predicted by oyster reef exposure to wind-driven waves, as measured by the Relative Exposure Index (REI) ($P = 0.012$, $R^2 = 0.38$; Fig. 2*B* and *SI Appendix*, Table S2). Of the 91 oyster reefs that fully converted

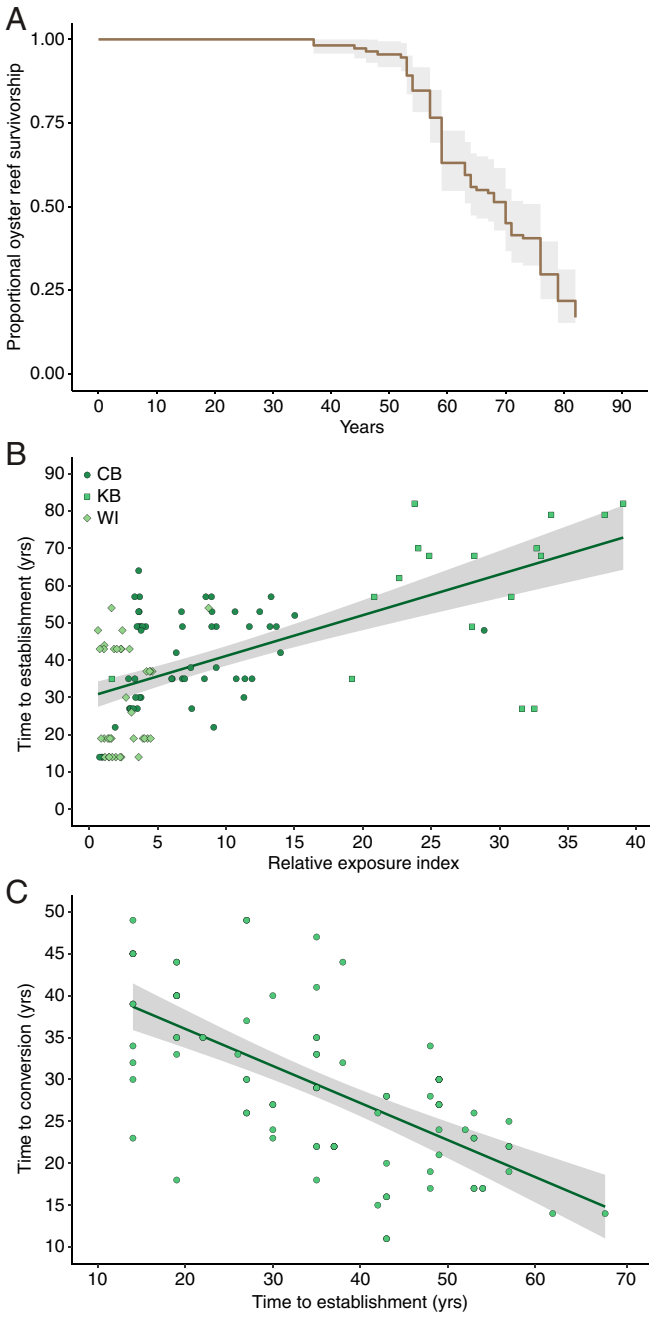

Fig. 2. Dynamics of oyster reef–to–mangrove transition spanning 82 y in Tampa Bay, FL, USA. (*A*) Over 80% of tracked oyster reefs fully converted (≥ 90% mangrove cover) to mangrove islands by 2020 (n = 111). (*B*) Physical exposure expressed as REI best predicted time to mangrove establishment across the three sites (*SI Appendix*, Table S2) and (*C*) conversion time of oyster reef–to–mangrove islands decreased over 82 y as time to establishment increased (*SI Appendix*, Table S3). CB, Cockroach Bay; KB, Kitchen Bayou; WI, Weedon Island.

to mangrove islands, mean (± SD) time to conversion was 29.1 ± 9.6 y, with the shortest and longest conversion times being 11 and 49 y, respectively. Distance to nearest mangrove, site, and time to mangrove establishment were significant predictors of time to conversion; however, only time to establishment possessed a high coefficient of determination ($P < 0.001$, $R^2 = 0.43$; Fig. 2*C* and *SI Appendix*, Table S3). Notably, time to conversion decreased as a function of time to establishment, indicating oyster reef–to–mangrove regime shifts increased in rate over the last 40 y (Fig. 2*C*).

Scrutiny of climate records suggests decreasing conversion times of oyster reefs (Fig. 2*C*) can be explained by contemporary increases in annual minimum temperature (T_{min}) and subsequent expansion of mangroves on oyster reefs. Structural-change analysis of climate data indicated no shifts in rainfall over the study duration but identified a 30-y cold period from 1956 to 1986 characterized by a T_{min} of −2.9 ± 2.1 °C (mean ± SD) and two freeze events with minimum temperatures below −7.3 °C, the physiological tolerance limit that has been experimentally estimated for the red mangrove (17) (Fig. 3). A release from severe freeze events after 1986 (Fig. 3*B*) corresponded with a change in slope of proportional mangrove area on oyster reefs after 1989 (Fig. 3*A*). Thus, oyster reefs that experienced mangrove establishment prior to 1986 took 33.3 ± 8.6 (mean ± SD) y to convert fully to a mangrove state and more than a decade longer than oyster reefs where mangroves established after 1986 (22.4 ± 8.6 [mean ± SD] y; degrees of freedom = 88.2, $t = 6.896$, $P < 0.001$).

Freeze events below −7.3 °C were linked to reduced mangrove cover on oyster reefs, but impacts were site dependent and related to microclimate (Fig. 3*A*). Mangrove cover decreased at the highly exposed Kitchen Bayou site between 1980 and 1987, while the rate of mangrove expansion slowed at Weedon Island, the most northern site (Fig. 3*A*). Both locations showed evidence of freeze impacts in aerial imagery (*SI Appendix*, Fig. S1*A* and *B*). The rate of proportional mangrove area increase was unchanged over the same period at Cockroach Bay (Fig. 2*A*), with the nearest weather station recording a T_{min} of −5.6 °C and little evidence of freeze impacts in aerial imagery (*SI Appendix*, Fig. S1*C*). These observations corroborate previous work suggesting that localized mangrove damage during freeze events is modulated by microclimate, with more exposed sites at greater risk of freeze impacts (21).

In situ surveys, sediment cores, and radiocarbon dates of underlying reef formation suggest a novel ecosystem state was reached following mangrove conversion and that such transitions are abrupt. Radiocarbon dates within cores and at the base of oyster reef strata show these habitats existed for centuries prior to conversion, making oyster reef–to–mangrove transitions appropriately categorized as "abrupt"—on the order of decades and recorded most frequently in the last 30 y (Fig. 4 and *SI Appendix*, Fig. S2). Benthic assessments from the center of converted mangrove islands showed few live oysters (81 ± 118 [mean ± SD] oysters m^{-2}), with densities orders of magnitude lower than those reported on oyster reefs from separate studies in Tampa Bay, FL (345 ± 44 [mean ± SD] oysters m^{-2}; 1,068 ± 744 [mean ± SD] oysters m^{-2}] (22, 23). Shifts in ecosystem state were also recorded in sediment properties, with an increase in percent total organic matter and accumulation of fine-grain sediments concomitant with mangrove expansion (Fig. 4*A*). Such characteristics of mangrove island formation are in stark contrast to $CaCO_3$ values exceeding 10% in oyster reef core strata preceding mangrove establishment (Fig. 4*A* and *B*) or typical of extant oyster reefs (Fig. 4*C*). Sedimentation is a well-known source of oyster mortality (24), and our data not only provide evidence that a novel state is reached following mangrove island formation but they also suggest a mechanism by which mangroves displace oysters through burial and eventually increase surface elevation (25), likely above oyster desiccation limits.

Climate models from near the current latitudinal range limit for mangroves suggest that historical trends in transition dynamics observed in Tampa Bay should expand poleward this century if propagule supply keeps pace with predicted warming. Statistically downscaled and bias-corrected Coupled Model Intercomparison Project (CMIP5) models of annual T_{min} at

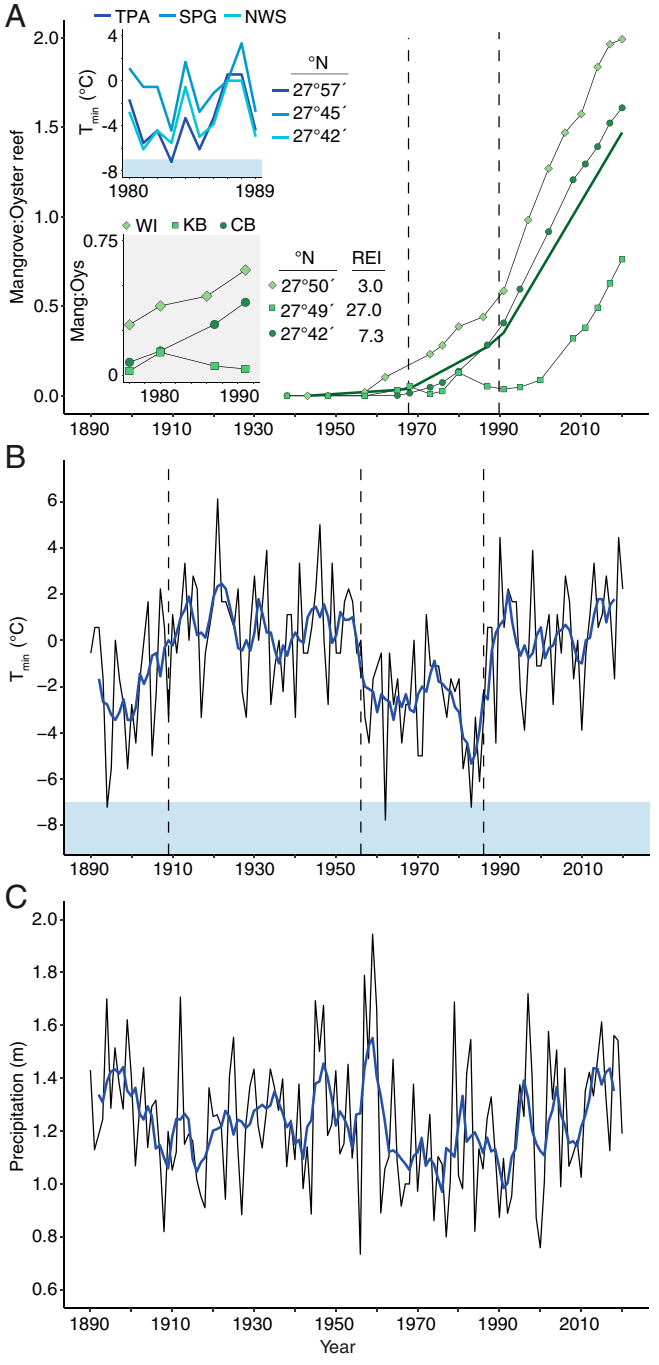

Fig. 3. Relationship between mangrove expansion on oyster reefs and climate. (*A*) Proportional change in mangrove cover relative to initial oyster reef area across three sites: Cockroach Bay (CB), Kitchen Bayou (KB), and Weedon Island (WI). Solid dark green line represents best-fit segmented regression for mangrove expansion across all sites. *Insets* show T_{min} at three weather stations (see Fig. 1*A*) and changes in proportional mangrove cover by site before and after the 1983 freeze. Latitudes (°N) of stations and sites are listed, along with mean oyster reef REI at each site. (*B*) Annual minimum temperature (T_{min}) and (*C*) annual precipitation in Tampa, FL, since 1890. Solid blue lines show 5-y moving averages. Light blue areas in (*B*) indicate freezing temperatures below -7.3 °C which is considered lethal to mangroves. Dashed vertical lines in *A* and *B* show estimated structural changes in timeseries; no structural changes were identified in *C*. Mang, mangrove; NWS, National Weather Service; Oys, oyster; SPG, Albert Whitted Airport (St. Petersburg); TPA, Tampa International Airport.

Cedar Key, FL, reveal that mean annual T_{min} is projected to reach between 0.5 and 1.7 °C by 2100, more than 3 °C warmer than the observed mean T_{min} of −2.6 °C between 1950 and 2005 (Fig. 5). Although minor freezes will still be common through the end of 2100, model realizations under both Representative Concentration Pathway (RCP) scenarios show that severe freezes below the red mangrove tolerance limit will become increasingly rare after 2070 (Fig. 5). If model predictions from even the moderate climate warming scenario are realized (Fig. 5*B*), mangrove release from extreme freezes should be expected between Tampa and Cedar Key within the next 50 y, putting extensive oyster habitat (26) in jeopardy of regime shifts by encroaching mangroves.

Although numerous studies have acknowledged the transgression of oyster reefs to mangrove islands over geologic timescales (27, 28), the suggestion that oyster reef replacement by mangroves is climate mediated has only recently been offered (29). Our results build upon this work by adding that oyster reef–to–mangrove transitions constitute regime shifts since they are abrupt, persistent in the face of periodic historical freezes, and undergo dramatic shifts in ecosystem structure. We also identify important, nonclimate-mediated drivers of ecosystem change that were previously unexplored. Specifically, establishment of mangroves on oyster reefs is strongly influenced by exposure to wind-driven waves and is consistent with previous work also identifying hydrodynamic force as a source of propagule disturbance (30).

A key finding that emerged from our historical analyses is that the well-described regime shift in tidal wetlands does not exist in isolation but cascades to nearby oyster reefs. The coupling of regime shifts results from the building supply of mangrove propagules in adjacent tidal wetlands. As the historical conversion of tidal wetlands proceeded along Tampa Bay coastlines, mangrove propagules became available to disperse with water currents and be intercepted by oyster reefs, which have no prior seed bank (Fig. 1*C*). The coupling of regime shifts linked to provision of propagules is reflected in a comparison of transition timelines. In Tampa Bay, mangroves largely displaced salt marshes prior to the 1980s and dominated large areas of coastline prior to the rapid expansion of mangrove proportional cover on oyster reefs from 1990 to the present (19, 20) (Fig. 3*A* and *SI Appendix*, Fig. S3). We also observed markedly lower proportional mangrove cover on centuries-old oyster reefs from 1930 to 1950, despite similar climate conditions (i.e., lack of freezes) that allowed for the rapid expansion of mangroves on oyster reefs recorded after 1990 (Fig. 3*A* and *B*). Assuming constant marsh-to-mangrove conversion rates provided by Raabe et al. (19), tidal wetlands near our study sites ranged from 30 to 60% conversion by 1950 (*SI Appendix*, Fig. S4). Thus, propagule supply pre-1950 may simply have been insufficient to sustain the oyster reef–to–mangrove regime shift during suitable climate conditions. Coupling via propagule dispersal is further supported by our finding of distance to nearest mangrove being a significant predictor of time to mangrove conversion of oyster reefs (*SI Appendix*, Table S3) and is aligned with studies of red mangrove dispersal documenting higher density of red mangrove propagules arriving at sites closer to release locations (31, 32). Overall, our findings suggest a model of multiple tipping dynamics, where climate first drives mangrove displacement of adjacent tidal marsh and, as mangrove proportional dominance increases in wetlands, an accompanying increase of external propagule supply eventually cascades in either a domino, two-phase cascade or joint cascade onto oyster reefs (sensu refs. 13 and 15).

This study adds to an increasing body of work that forecasts landscape-wide changes in estuaries this century (18, 33–36). Ecosystem structure and function will become increasingly tropical in temperate zones as climate warms (36), with the type and

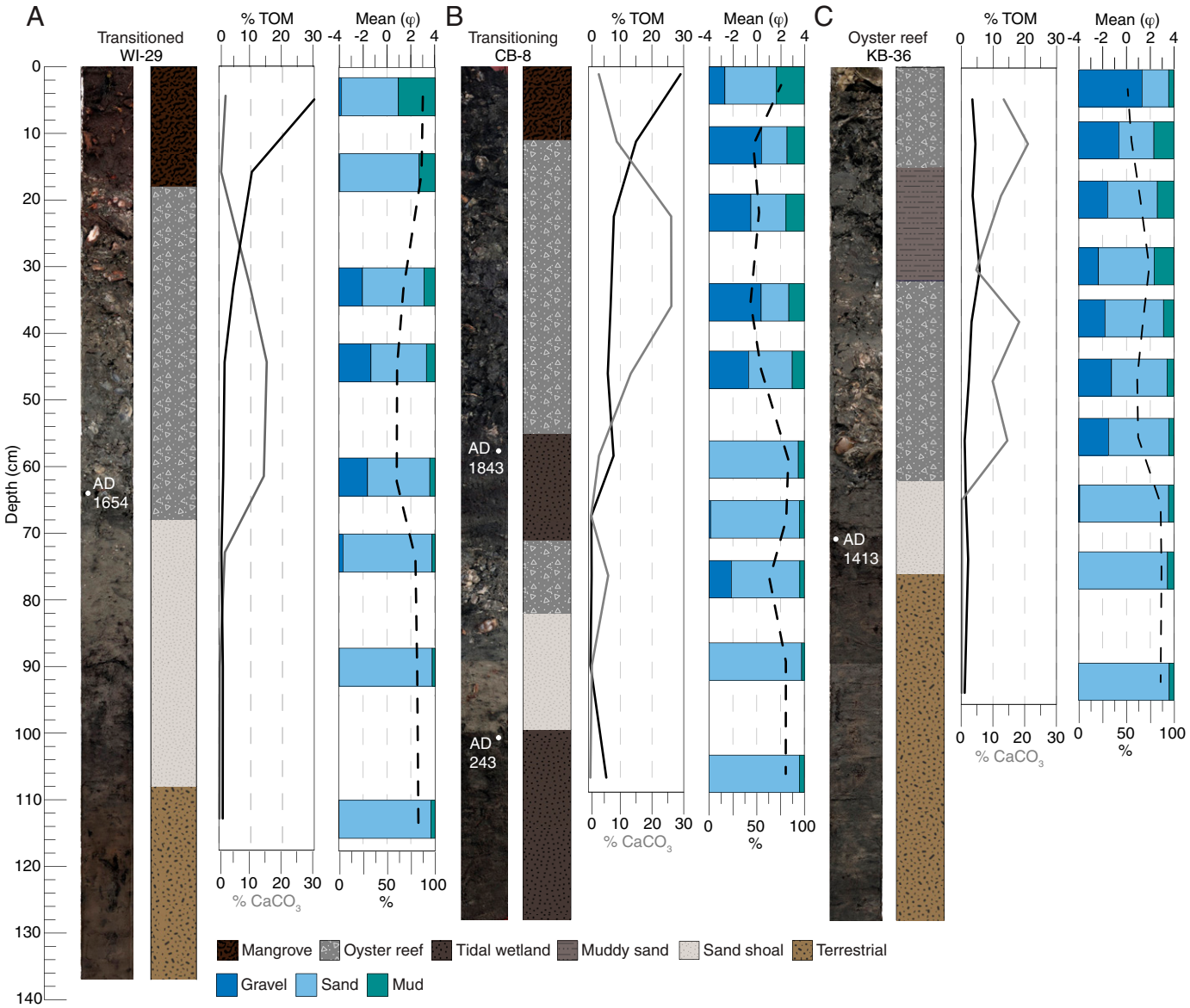

Fig. 4. Sediment cores showing (*A*) a fully transitioned mangrove island, (*B*) an oyster reef undergoing transition, and (*C*) an extant oyster reef. Stratigraphy was described through visual inspection and sediment properties, including percent total organic matter (% TOM), % $CaCO_3$, and grain-size analyses. Dotted line shows mean grain size (φ). White dots show locations of accelerator mass spectrometry radiocarbon dating of macrobotanical or charcoal elements. Dates represent median age probabilities. See *SI Appendix*, Fig. S2 for additional cores and radiocarbon dates from converted mangrove islands.

availability of ecosystem goods and services altered in estuaries with historically temperate-species assemblages (37, 38). Although mangrove forests provide a suite of valued ecosystem services, such as carbon sequestration and land formation (39), other ecosystem functions unique to oyster reefs will be diminished or lost altogether. For instance, oyster reef–to–mangrove regime shifts directly threaten wild oyster fisheries and reef-dependent species, such as the American oystercatcher (*Haematopus palliates*) (40), between Tampa and Cedar Key through loss of habitat. If mangrove propagule dispersal poleward keeps pace with the climate projections we report here, managers will encounter these tradeoffs within decades.

From Tampa Bay southward, oyster reef transition to mangrove forest is well advanced (e.g., Ten Thousand Islands), but for areas northward that are dominated by herbaceous tidal wetlands, oyster reef conversion remains a probable future. Our study provides potential pathways to address challenges associated with this climate-mediated, cascading regime shift depending upon management goals (6). For example, if transition to mangrove is desired, then we present a timetable during which an anticipated date for mangrove conversion of oyster reefs could be incorporated into regional plans. Alternatively, human actions could intervene if oyster reef resilience is preferred. Given that mangrove establishment is dependent upon propagule capture by oyster reefs, multiple tipping dynamics could be disrupted by weeding of early established propagules or even removal of saplings from reefs. Likewise, our study identified oyster reef resilience to mangrove conversion could be increased by selecting settings for reef restoration in coastal waters within which the upper limit of natural oyster reef exposure is found (41). In the absence of such human interventions, the climate-driven, coupled regime shifts we outline here run the risk of homogenizing subtropical landscapes over this century.

Materials and Methods

Study Area. Tampa Bay, FL, is a subtropical estuary on Florida's Gulf coast spanning more than 1,000 km^2 between latitudes 27°30′00″ and 28°00′00″ N

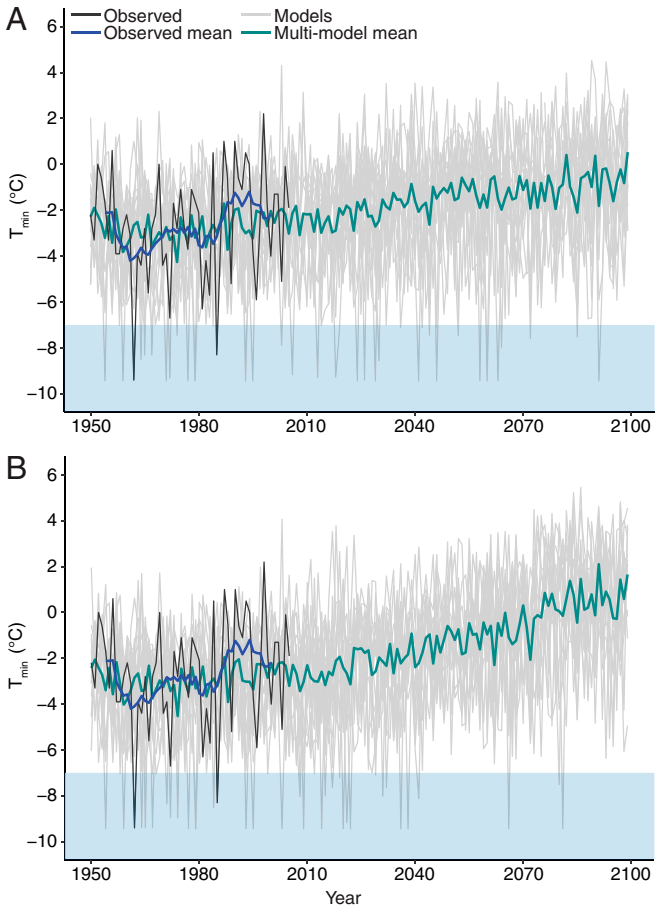

Fig. 5. T_{min} data through 2099 at Cedar Key, FL, under two radiative forcing scenarios: (*A*) RCP4.5 and (*B*) RCP8.5. Black lines are historical observations and the dark blue line represents 5-y moving average for historical data. Light gray lines are individual CMIP5 model realizations; the multimodel mean is in teal. Light blue areas on temperature graphs indicate freezes below −7.3 °C.

(Fig. 1*A*) (42, 43). Mean depth is 3.3 m and the microtidal system oscillates between diurnal and mixed-semidiurnal tides (42). Salinity can range widely from 2 to 35 psu and varies spatially and temporally depending upon proximity to freshwater sources and with the pronounced winter-dry and summer-wet periods (42). The shoreline and surrounding watershed are heavily urbanized (43), with extensive coastal modification beginning in the mid-20th century (20). Remnant shorelines and shallow coastal waters support typical subtropical marine habitats, including mangrove forests, salt marshes, seagrass beds, oyster reefs, mud flats, and macroalgal patches (42, 43).

Within Tampa Bay, three study sites were selected to examine past oyster reef–to–mangrove transition: Weedon Island, Kitchen Bayou, and Cockroach Bay (Fig. 1*A*). Study sites were selected based upon their limited shoreline development and the continuity of aerial imagery being available from 1938 to present. Each study site possesses a mangrove-dominated shoreline, a patchwork of oyster reefs (with and without mangroves), and mangrove islands. Based upon field surveys, *R. mangle* is dominant species of vegetation on mangrove islands in our study area.

Aerial Imagery. Historical aerial monochromatic and color satellite images were compiled for each study site from 1938 to 2020 (*SI Appendix*, Table S1). We included imagery at decadal intervals through the 1950s and twice per decade after 1960. Monochrome aerials were manually georeferenced to recent satellite imagery using, at minimum, three control points. Raster image quality ranged from 1.46- to 0.15-m resolution, which allowed sufficient interpretation of underlying features in both monochrome and color images. All aerial imagery was curated, and subsequent analysis conducted, in ArcGIS Pro-2.4.0.

To examine dynamics of oyster reef–to–mangrove transition from aerial imagery, all oyster reefs without mangroves in the first available imagery at each site were followed through time and aspects of mangrove conversion recorded ($n = 111$). Oyster reef features were distinguished from surrounding benthic habitats by their ovate to linear shape and brighter (more reflective) signatures than surrounding benthic habitats. Mangrove canopies contrast sharply with oyster reef features and appear as dark-colored dots or clumps in black-and-white photographs (Fig. 1*B*). Features were hand digitized from underlying georeferenced imagery, including initial oyster reef area in 1938 or 1943 (depending upon site, see *SI Appendix*, Table S1), mangrove area on each oyster reef and at each time point, and the total feature area at each time point (area of oyster reef plus any mangrove area). Digitized mangrove area was used to identify the year a mangrove was first observed on an oyster reef, whether an oyster reef fully converted to a mangrove island, and the year full conversion was reached. Full transition of an oyster reef to mangrove state was defined as ≥ 90% mangrove cover relative to the total area of the feature at each time point.

Observations of oyster reef to mangrove transition were used to determine 1) time to establishment, 2) time to conversion, and 3) proportional mangrove area of converted reefs. Time to establishment was defined as the difference in years between the first observation of mangrove presence on an oyster reef and the year of initial imagery (*SI Appendix*, Table S1). Time to conversion was defined as the number of years between the date of first mangrove establishment and date of full conversion. We quantified proportional mangrove area as the total area of mangroves on oyster reefs standardized to the initial oyster reef area at each site. Standardizing mangrove area to starting oyster reef area allowed for comparison of expansion across sites; however, values can exceed 1.0 due to expansion of oyster reef area followed by eventual mangrove takeover or additional areal expansion due to mangrove "land building." Given the resolution of monochrome images was <1.5 m, mangroves could not be detected until the sapling life stage. Mean (± SD) mangrove canopy width at detection was 1.24 ± 0.59 m. Thus, time to establishment and conversion metrics are underestimated by at least 2 to 3 y.

Two aspects of physical setting–distance to nearest mangrove and exposure to wind-driven waves–were also quantified for each oyster reef using initial imagery at each site. Distance to the nearest mangrove was calculated as the linear distance from the centroid of an oyster reef to the closest mangrove (either on another reef or the coastline). Exposure was estimated using the REI, which calculates a dimensionless value of wind-driven wave energy based upon a point location's effective fetch, average wind speed, and percent direction (44). To calculate REI, oyster reef centroids were used to measure the direct fetch distance to the nearest shoreline along an array of 36 lines separated by 10° increments. Only landforms with features above mean sea level (e.g., mainland, barrier islands, tidal wetlands, mangrove islands), not adjacent oyster reefs, were considered to possess shoreline and, therefore, obstructions to wind-driven waves. Effective fetch was then calculated using the following equation:

$$F_i = \sum_{n=1}^{5} y_n \times \cos(x_i), \quad [1]$$

where y_n is the direct fetch and x_i is the angle of departure from the *i*th compass heading. Effective fetch along the *i*th heading for each oyster reef was then combined with measurements of wind speed and direction recorded at the Tampa International Airport (station identifier [ID]: USW00012842) from 1965 to 2020 to calculate REI for an individual oyster reef. Daily measurements of average 1 or 2-min wind speed and direction were obtained from the National Centers for Environmental Information (NCEI) of the National Oceanic and Atmospheric Administration (NOAA), and the 5% fastest speeds over the observation period were extracted for analysis. REI was calculated using the following equation:

$$REI = \sum_{i=1}^{32} (V \times P_i \times F_i), \quad [2]$$

where V is average wind speed, P_i is the proportion of wind speeds along the *i*th compass heading, and F_i is effective fetch along the *i*th compass heading. REI is only useful in comparing relative differences in exposure between locations or sites calculated in a similar way and from the same study.

Historical Climate Data. To examine the influence of local climate on oyster reef–to–mangrove transition, temperature and precipitation records from 1890 to 2020 were compiled for Tampa, FL. Daily observations were obtained from the NCEI (station IDs: USC00088786, USW00012842) and annual records from

the Florida Climate Data Center (FCDC). Daily observations were used to calculate annual minimum temperature (T_{min}) and precipitation for years not available from the FCDC. Annual minimum temperature represents the coldest recorded temperature in the year. Previous studies have shown this metric predicts mangrove presence and expansion at the eastern North American range limit (16, 17, 33). Annual precipitation was calculated as the sum of rainfall totals over the year. We included precipitation due to its influence on red mangrove phenology (45) and limitation at certain range limits (16). Annual T_{min} was also obtained for local weather stations near field sites during the 1980s (station IDs: USC00088782, USC00087886) (Fig. 1*A*).

Field Surveys and Sediment Cores. Live oyster densities underneath mangrove canopies were quantified to assess whether fully converted mangrove islands have oyster densities comparable to natural reefs. A 0.25-m^2 quadrat was placed at the approximate center of six randomly selected mangrove islands at each study site. Surface shell and any oysters on prop roots were removed from each quadrat and live oysters counted to estimate density. Live oyster densities underneath mangrove canopies were compared with previously published values of live oyster densities on reefs in Tampa Bay (22, 23).

Sediment cores were collected from extant features to examine whether recent mangrove island formation on oyster reefs is reflected in the sedimentary record. At each study site, core samples were taken at two mangrove islands historically classified as oyster reef. Additional cores were collected at Cockroach Bay and Kitchen Bayou sites from within the mangrove canopy of a mostly transitioned oyster reef (67% mangrove cover) and an extant oyster reef that lost mangrove cover over the 20th century due to freezes. Core samples were driven into the subsurface by manual percussion, fitted with an air-tight stopper, and extracted. Cores were collected in aluminum tubes measuring 7.6 cm in diameter and ∼2 m in length. Core penetration depths and compaction rates were measured in the field and utilized to produce compaction-corrected core logs.

Core samples were split, photographed, and described initially through qualitative assessment of sedimentary characteristics, such as texture, structure, coloration, contact boundaries, and macrofossil composition. The two cores from a mostly transitioned oyster reef at Cockroach Bay and extant oyster reef at Kitchen Bayou were subsampled stratigraphically for quantitative sediment analysis, enabling the characterization of sedimentary units and identification of different depositional environments. For sediment grain-size analysis, samples were disbursed, wet sieved through 63-μm mesh, and dried at 80 °C to obtain mud fractions. Coarse fractions (>63 μm) were dried and processed through nested brass sieves ranging from −4.25 phi to 4 phi at 0.25-phi intervals and used to estimate mean grain size and percent gravel (>2 mm), and percent sand (2 mm to 63 μm). Total organic matter and $CaCO_3$ content were estimated through loss on ignition at 550 °C and 900 °C, respectively, for 5 h. Additionally, we collected five total macrobotanical or charcoal elements from the four cores for accelerator mass spectrometry radiocarbon analysis at the Center for Applied Isotope Studies at the University of Georgia (Athens, GA).

Climate Simulations. We examined global climate model (GCM) data from the CMIP5 to predict when oyster reefs could become vulnerable to rapid mangrove transition at Cedar Key, FL, near the poleward range limit for the red mangrove (*R. mangle*) on Florida's Gulf coast (29°10′00″ N) (16) (Fig. 1*A*). Daily minimum temperature for a 4-km grid overlapping Cedar Key was extracted from 16 GCMs from the same CMIP5 ensemble and downscaled using the multivariate adaptive constructed analogs method (46). GCMs included a 1950 to 2005 historical scenario, driven by past solar radiation, atmospheric conditions, and greenhouse gas concentrations, as well as a 2006 to 2099 simulation under either a moderate radiative forcing projection, RCP4.5, or an aggressive scenario (RCP8.5). RCP4.5 is expected to either be a less-than-realistic or realistic scenario resulting from estimated future emissions by midcentury, although recent emissions track RCP8.5 (47, 48).

Temperature observations from Cedar Key, FL, were used to correct GCM historical and future simulations. Daily temperature records from 1950 to 2005 were obtained from NOAA's NCEI (station ID: USC00081432) as well as the National Data Buoy Center (station ID: CDRF1). Daily minimum temperature was directly recorded at weather stations and daily average temperate was calculated as the midpoint between daily minimum and maximum temperatures. Missing records at Cedar Key were gap filled using the correlation with temperature records from nearby Gainesville, FL (station IDs: USC00083316, USW00012816). All GCM outputs were then bias corrected using the observation record for annual minimum temperature:

$$\mathrm{GCM}_{BC}(t) = \overline{\mathrm{Obs}_{REF}} + \frac{\sigma_{\mathrm{Obs}_{REF}}}{\sigma_{\mathrm{GCM}_{REF}}}\left(\mathrm{GCM}_{RAW}(t) - \overline{\mathrm{GCM}_{REF}}\right), \quad [3]$$

where GCM_{BC} are the bias corrected GCM temperature data, Obs_{REF} are the historical temperature records during the 1950 to 2005 reference period, GCM_{REF} are the raw GCM data during that same historical reference period, and GCM_{RAW} are the raw GCM temperature data from both historical and future scenarios.

Daily minimum temperature estimates were further quantile mapped using the package *qmap*. Quantile mapping uses the cumulative distribution function from the historical reference period (1950 to 2005) to create the same temporal distribution of simulated minimum temperature values but restricted to the historical distribution. Thus, as climate warms, quantile mapping underestimates simulated minimum temperature (18). However, since historical freezes in Cedar Key exceeded the red mangrove temperature physiological threshold (15, 16), this artifact of quantile mapping does not alter our conclusions of future extreme events in the context of mangrove expansion on oyster reefs.

To predict when climate will become conducive to oyster reef transition in Cedar Key, daily calibrated GCM data were used to construct models of future annual minimum (T_{min}) and examined in the context of extreme freeze events observed to influence regime shifts in Tampa Bay. Annual T_{min} is defined as the lowest simulated temperature observed in a year. Multimodel means were calculated by averaging across all 16 individual GCMs for a particular year and RCP. Although we use GCMs to identify future periods at Cedar Key where severe freezes below –7.3 °C become increasingly rare, it should be noted that such models are limited in their ability to predict extreme events at local scales, due to their initial resolution and inability to capture all influences on regional climate (18).

Statistical Analysis. Dynamics of oyster reef–to–mangrove transition were described using a combination of statistical models and structural change analysis of time series. Oyster reef transition over the 82-y study period was first modeled as a Kaplan-Meier survival response (1 = converted, 0 = not converted; $n = 111$) using the R package *survival*. For the oyster reefs where mangroves established ($n = 108$), we used a linear model to test whether REI, site, initial oyster reef area, and distance to nearest mangrove predicted time to establishment. In a separate linear model, we examined whether oyster reefs that fully converted ($n = 91$) were influenced by REI, site, initial oyster reef area, distance to nearest mangrove, or the year of mangrove establishment.

Structural-change analysis was used to identify shifts in climate time series from Tampa Bay, which were related to observed changes in mangrove expansion on oyster reefs. Breakpoints in annual temperature and precipitation data were computed using the R package *strucchange*, which identifies moments of structural change in time series through minimizing the residual sum of squares in multiple regression segments. We report the minimum number of breakpoints while maximizing reductions in residual sum of squares. We also applied segmented regression analysis to time series of proportional mangrove area on oyster reefs using the R package *segmented*.

Data Availability. All data are included in the manuscript and/or supporting information (*SI Appendix*, Datasets S1).

ACKNOWLEDGMENTS. We thank N. S. Mathews for assisting with fieldwork, B. T. Furman for thoughtful and constructive comments on the manuscript, and A. Huse at University of South Florida Special Collections for assistance with historical photographs. This work was made possible by funding from the Fred L. & Helen M. Tharp Endowment Scholarship and the NSF (15-554 Archaeology Program, Grant 2024397, principal investigators: T. Pluckhahn, K.J.). Live oysters were sampled under the Florida Fish & Wildlife Conservation Commission special activity license (SAL-19-1633-SR).

Author affiliations: [a]Department of Integrative Biology, University of South Florida, Tampa, FL, 33620; and [b]Department of Anthropology, University of South Florida, Tampa, FL, 33620

1. M. Scheffer, S. R. Carpenter, Catastrophic regime shifts in ecosystems: Linking theory to observation. *Trends Ecol. Evol.* **18**, 648–656 (2003).
2. R. Biggs, G. Peterson, J. Rocha, The Regime Shifts Database: A framework for analyzing regime shifts in social-ecological systems. *Ecol. Soc.* **23**, art9 (2018).
3. A. D. Barnosky *et al.*, Approaching a state shift in Earth's biosphere. *Nature* **486**, 52–58 (2012).
4. E. H. van Nes *et al.*, What do you mean, 'tipping point'? *Trends Ecol. Evol.* **31**, 902–904 (2016).
5. N. A. J. Graham *et al.*, Managing resilience to reverse phase shifts in coral reefs. *Front. Ecol. Environ.* **11**, 541–548 (2013).
6. S. T. Jackson, Transformational ecology and climate change. *Science* **373**, 1085–1086 (2021).
7. S. Drijfhout *et al.*, Catalogue of abrupt shifts in Intergovernmental Panel on Climate Change climate models. *Proc. Natl. Acad. Sci. U.S.A.* **112**, E5777–E5786 (2015).
8. C. H. Trisos, C. Merow, A. L. Pigot, The projected timing of abrupt ecological disruption from climate change. *Nature* **580**, 496–501 (2020).
9. P. D. Wallingford *et al.*, Adjusting the lens of invasion biology to focus on the impacts of climate-driven range shifts. *Nat. Clim. Chang.* **10**, 398–405 (2020).
10. J. Sheridan, D. Bickford, Shrinking body size as an ecological response to climate change. *Nat. Clim. Chang.* **1**, 401–406 (2011).
11. D. P. Tittensor *et al.*, Next-generation ensemble projections reveal higher climate risks for marine ecosystems. *Nat. Clim. Chang.* **11**, 973–981 (2021).
12. J. C. Rocha, G. D. Peterson, R. Biggs, Regime shifts in the Anthropocene: Drivers, risks, and resilience. *PLoS One* **10**, e0134639 (2015).
13. J. C. Rocha, G. Peterson, Ö. Bodin, S. Levin, Cascading regime shifts within and across scales. *Science* **362**, 1379–1383 (2018).
14. M. G. Turner *et al.*, Climate change, ecosystems and abrupt change: Science priorities. *Philos. Trans. R. Soc. Lond. B Biol. Sci.* **375**, 20190105 (2020).
15. A. K. Klose, N. Wunderling, R. Winkelmann, J. F. Donges, What do we mean, 'tipping cascade'? *Environ. Res. Lett.* **16**, 125011 (2021).
16. M. J. Osland *et al.*, Climatic controls on the global distribution, abundance, and species richness of mangrove forests. *Ecol. Monogr.* **87**, 341–359 (2017).
17. R. Bardou, J. D. Parker, I. C. Feller, K. C. Cavanaugh, Variability in the fundamental versus realized niches of North American mangroves. *J. Biogeogr.* **48**, 1–16 (2020).
18. K. C. Cavanaugh *et al.*, Climate-driven regime shifts in a mangrove-salt marsh ecotone over the past 250 years. *Proc. Natl. Acad. Sci. U.S.A.* **116**, 21602–21608 (2019).
19. E. A. Raabe, L. C. Roy, C. C. McIvor, Tampa Bay coastal wetlands: Nineteenth to twentieth century tidal marsh-to-mangrove conversion. *Estuaries Coast* **35**, 1145–1162 (2012).
20. K. Jackson, G. R. Brooks, R. A. Larson, Of marsh and mangrove: Coupled biophysical and anthropogenic drivers of 20th century wetland conversion in Tampa Bay Estuary, Florida (USA). *Anthropocene* **34**, 100295 (2021).
21. M. J. Osland *et al.*, Microclimate influences mangrove freeze damage: Implications for range expansion in response to changing macroclimate. *Estuaries Coast* **42**, 1084–1096 (2019).
22. M. L. Parker, W. S. Arnold, S. P. Geiger, P. Gorman, E. H. Leone, Impacts of freshwater management activities on eastern oyster (*Crassostrea virginica*) density and recruitment: Recovery and long-term stability in seven Florida estuaries. *J. Shellfish Res.* **32**, 695–708 (2013).
23. M. Drexler, M. L. Parker, S. P. Geiger, W. S. Arnold, P. Hallock, Biological assessment of eastern oysters (*Crassostrea virginica*) inhabiting reef, mangrove, seawall, and restoration substrates. *Estuaries Coast* **37**, 962–972 (2014).
24. A. M. Colden, R. N. Lipcius, Lethal and sublethal effects of sediment burial on the eastern oyster *Crassostrea virginica*. *Mar. Ecol. Prog. Ser.* **527**, 105–117 (2015).
25. G. A. Coldren, J. A. Langley, I. C. Feller, S. K. Chapman, Warming accelerates mangrove expansion and surface elevation gain in a subtropical wetland. *J. Ecol.* **107**, 79–90 (2019).
26. J. R. Seavey, W. E. Pine III, P. Frederick, L. Sturmer, M. Berrigan, Decadal changes in oyster reefs in the Big Bend of Florida's Gulf coast. *Ecosphere* **2**, 1–14 (2011).
27. R. W. Parkinson, Decelerating Holocene sea-level rise and its influence on southwest Florida coastal evolution: A transgressive/regressive stratigraphy. *J. Sediment. Petrol.* **59**, 960–972 (1989).
28. D. R. Cahoon, J. C. Lynch, Vertical accretion and shallow subsidence in a mangrove forest of southwestern Florida, U.S.A. *Mangroves Salt Marshes* **1**, 173–186 (1997).
29. G. McClenachan, M. Witt, L. J. Walters, Replacement of oyster reefs by mangroves: Unexpected climate-driven ecosystem shifts. *Glob. Change Biol.* **27**, 1226–1238 (2021).
30. T. Balke *et al.*, Cross-shore gradients of physical disturbance in mangroves: Implications for seedling establishment. *Biogeosciences* **10**, 5411–5419 (2013).
31. R. Sengupta *et al.*, Landscape charactertistics of *Rhizophora mangle* forests and propagule deposition in coastal environments of Florida (USA). *Landsc. Ecol.* **20**, 63–72 (2007).
32. N. Goldberg, J. N. Heine, Life on the leading edge: Phenology and demography of the red mangrove *Rhizophora mangle* L. at the northern limit of its expanding range. *Flora* **235**, 76–82 (2017).
33. K. C. Cavanaugh *et al.*, Poleward expansion of mangroves is a threshold response to decreased frequency of extreme cold events. *Proc. Natl. Acad. Sci. U.S.A.* **111**, 723–727 (2014).
34. C. A. Gabler *et al.*, Macroclimatic change expected to transform coastal wetland ecosystems this century. *Nat. Clim. Chang.* **7**, 143–147 (2017).
35. M. L. Kirwan, K. B. Geden, Sea-level driven land conversion and the formation of ghost forests. *Nat. Clim. Chang.* **9**, 450–457 (2019).
36. M. J. Osland *et al.*, Tropicalization of temperate ecosystems in North America: The northward range expansion of tropical organisms in response to warming winter temperatures. *Glob. Change Biol.* **27**, 3009–3034 (2021).
37. J. J. Kelleway *et al.*, Review of the ecosystem service implications of mangrove encroachment into salt marshes. *Glob. Change Biol.* **23**, 3967–3983 (2017).
38. A. Armitage, C. A. Weaver, A. A. Whitt, S. C. Pennings, Effects of mangrove encroachment on tidal wetland plant, nekton, and bird communities in the Western Gulf of Mexico. *Estuar. Coast. Shelf Sci.* **248**, 106767 (2021).
39. S. Y. Lee *et al.*, Reassessment of mangrove ecosystem services. *Glob. Ecol. Biogeogr.* **23**, 726–743 (2014).
40. J. M. Brush, A. C. Schwarzer, P. C. Frederick, Importance and function of foraging and roost habitat for wintering American oystercatchers. *Estuaries Coast* **40**, 286–295 (2017).
41. S. J. Theuerkauf, D. B. Eggleston, B. J. Puckett, K. W. Theuerkauf, Wave exposure structures oyster distribution on natural intertidal reefs, but not on hardened shorelines. *Estuaries Coast* **40**, 376–386 (2017).
42. R. R. Lewis III, E. D. Estevez, "The ecology of Tampa Bay: An estuarine profile" (Biological Rep. 85:[7.18], U.S. Fish and Wildlife Service, Washington, DC, 1988).
43. Tampa Bay Estuary Program, "Tampa Bay Estuary Program: 2020 habitat master plan update" (Tech. Rep. #07-20, Tampa Bay Estuary Program, Tampa, FL, 2020).
44. L. A. Mason, C. M. Riseng, A. J. Layman, R. Jensen, Effective fetch and relative exposure index maps for the Laurentian Great Lakes. *Sci. Data* **5**, 180295 (2018).
45. J. R. Peel, J. Golubov, M. D. C. Mandujano-Sánchez, J. López-Portillo, Phenology and floral synchrony of *Rhizophora mangle* along a natural salinity gradient. *Biotropica* **51**, 355–363 (2019).
46. J. T. Abatzoglou, T. J. A. Brown, Comparison of statistical downscaling methods suited for wildfire applications. *Int. J. Climatol.* **32**, 772–780 (2012).
47. C. R. Schwalm, S. Glendon, P. B. Duffy, RCP8.5 tracks cumulative CO_2 emissions. *Proc. Natl. Acad. Sci. U.S.A.* **117**, 19656–19657 (2020).
48. Z. Hausfather, G. P. Peters, RCP8.5 is a problematic scenario for near-term emissions. *Proc. Natl. Acad. Sci. U.S.A.* **117**, 27791–27792 (2020).